DOI: 10.1002/ejic.200700972

Al-Doped Apatite-Type Nanocrystalline Lanthanum Silicates Prepared by Mechanochemical Synthesis: Phase, Structural and Microstructural Study

Tamara Kharlamova,*[a] Svetlana Pavlova,[a] Vladislav Sadykov,[a] Marina Chaikina,[b] Tamara Krieger,[a] Olga Lapina,[a] Dzhalil Khabibulin,[a] Arcady Ishchenko,[a] Vladimir Zaikovskii,[a] Christos Argirusis,[c] and Jorge Frade[d]

Keywords: Apatite-type silicates / Conducting materials / Doping / Mechanochemical synthesis / Formation mechanism

Al-doped $La_{9.33+x/3+y}Si_{6-x}Al_xO_{26+3y/2}$ (x = 0–1.5, y = 0–0.67) apatite-type lanthanum silicates (ATLS) were synthesized with a high-power (1200 rpm) planetary ball mill that allows the formation of the lanthanum silicate phase after milling for 20–35 min at room temperature. The apatite phase already appears after milling for 5 min. Phase, structural and microstructural studies on the nanocrystalline lanthanum silicates were carried out by using XRD, TEM, and IR, ^{27}Al and ^{29}Si MAS NMR spectroscopy to clarify the mechanism of ATLS formation. The cluster-topotactic mechanism of the formation of apatite by mechanochemical treatment involving hydration of the starting compounds and acid–base reactions is suggested. Al-doping results in promoting the formation of apatite. However, a secondary $LaAlO_3$ phase may be present in the sample depending on its stoichiometry. This suggests the existence of a biphase domain in the La_2O_3–SiO_2–Al_2O_3 phase diagram at room temperature, in which Al-doped apatite and $LaAlO_3$ phases coexist.

Introduction

Apatite-type lanthanum silicates (ATLS) have recently attracted considerable attention as oxygen ion conductors because of their high ionic conductivity at intermediate temperatures and low activation energy (4×10^{-3} S/cm at 500 °C and 0.6–0.8 eV).[1,2] These features are correlated with the crystal structure of such silicates. The hexagonal apatite structure belongs to the space group $P6_3/m$ or $P6_3$ and may be represented by the general unit-cell formula $M_{10}(RO_4)_6X_2$, where, in the case of ATLS, M is La or an alkaline earth ion, R is Si and X is an O ion.[3] It can be described as consisting of isolated tetrahedral RO_4 anions and M cations located in two non-equivalent sites – nine-coordinate 4f and seven-coordinate 6h sites (Figure 1). The latter forms channels that run through the structure in which the X anions are located. These channel anions are suggested to be responsible for the high ionic conductivity.

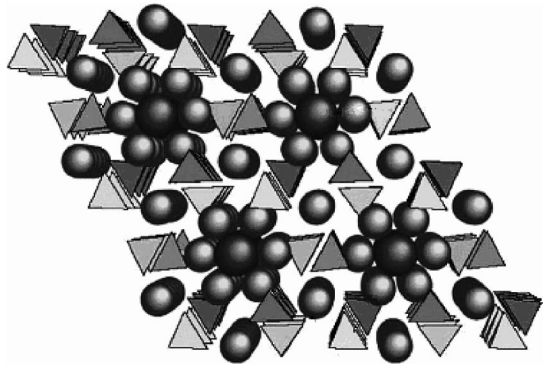

Figure 1. Structure of the apatite-type compounds, $M_{10}(RO_4)_6X_2$: RO_4 = tetrahedra, M = small spheres, X = big spheres.

The tolerance of the apatite lattice to M-site deficiency and extensive doping is one more particular feature of these apatite-type systems that provides an important tool for property optimization.[4] ATLS may have 6.7% vacancies in M sites, which is necessary to maintain charge neutrality of the compound. The amount of cation vacancies can be changed by doping, which may also be accompanied by the appearance of excess oxygen. It was shown that fully stoichiometric systems, such as $La_8Sr_2Si_6O_{26}$, have much lower conductivities and higher activation energies than those containing cation vacancies and/or oxygen excess.[3,4] In this respect, different doping strategies were proposed to increase the oxygen ion conductivity of ATLS.[4]

[a] Boreskov Institute of Catalysis SB RAS,
pr. Lavrentieva, 5, 630090 Novosibirsk, Russia
Fax: +7-383-3308056
kharlamova@catalysis.ru
[b] Institute of Solid State Chemistry and Mechanochemistry SB RAS,
Kutatetadze Street, 18, 630128 Novosibirsk, Russia
[c] Clausthal University of Technology,
38678 Clausthal-Zellerfeld, Germany
[d] University of Aveiro,
3810-193 Aveiro, Portugal

However, there are some challenges with regard to the synthesis and sintering that need to be solved to promote the application of ATLS.[3] The conventional synthesis of ATLS requires very long firing cycles at temperatures in the range 1200–1600 °C.[4,5] Further, temperatures in the range 1500–1700 °C are usually required to densify ATLS electrolytes.[5] Lower synthesis temperatures allow dispersed/nanocrystalline powders to be obtained, which play a crucial role in the sintering and densification of oxides.[6] Some low-temperature preparation methods such as sol-gel route or mechanochemical milling have been successfully used for the synthesis of undoped ATLS.[7,8]

Mechanical milling is widely used to synthesize nanocrystalline metals, powder alloys and novel crystalline phases.[6,9] It has also attracted great interest because of the possibility to carry out the syntheses at room temperature. Thus, Rodriguez-Reyna et al.[8] report that mechanical milling for 6 h with a moderate rotation speed (350 rpm) is sufficient to obtain a product consisting primarily of an undoped ATLS. However, Tzvetkov and Minkova[10] report that an amorphous precursor of lanthanum silicate oxyapatite was observed after milling of the starting SiO_2 and La_2O_3 mixture for 3 h at 256 rpm, and single-phase polycrystalline ATLS was obtained only after subsequent heating at 1000 °C for 2 h. In the present paper, the results of the mechanochemical synthesis of Al-doped $La_{9.33+x/3+y}Si_{6-x}Al_xO_{26+3y/2}$ (x = 0–1.5, y = 0–0.67) ATLS by using a high-power planetary ball mill are presented. Phase, structural and microstructural studies on the nanocrystalline lanthanum silicates were carried out to clarify the mechanism of their formation.

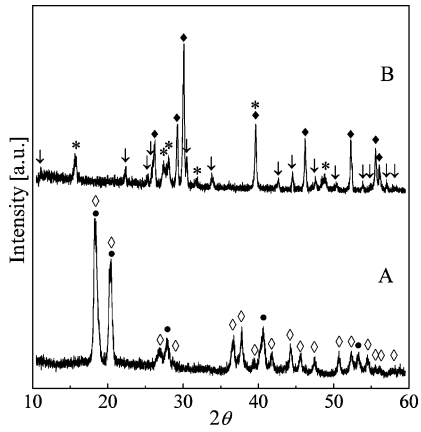

Figure 2. X-ray powder diffraction patterns of the parent compounds: (A) aluminum hydroxide, (B) lanthanum oxide; ✧ – gibbsite, ● – bayerite, ♦ – La_2O_3, * – $La(OH)_3$, ↓ – $La_2O_2CO_3$.

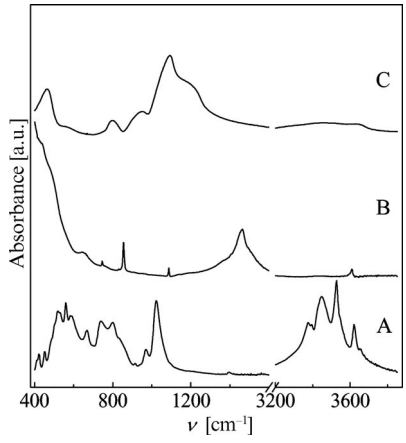

Figure 3. FTIR spectra of the parent compounds: (A) aluminum hydroxide, (B) lanthanum oxide, (C) silica.

Results and Discussion

Characterization of the Parent Compound

All parent compounds used here were characterized by XRD, IR spectroscopy and TG/DTA analysis. The XRD patterns and IR spectra of these reagents are presented in Figure 2 and Figure 3, respectively. According to the XRD data, admixtures of $La(OH)_3$ (PDF 36–1481) and $La_2O_2CO_3$ (PDF 37–0801) are present together with the initial lanthanum oxide and the hexagonal La_2O_3 phase (PDF 05–0602). This is confirmed by the corresponding IR spectrum: bands at 643 and 3610 cm^{-1} assigned to La–OH vibrations and those at 746, 853, 1089 and 1280–1650 cm^{-1} assigned to C–O vibrations in CO_3 group are observed. According to the XRD and IR data, the parent aluminium hydroxide is a mixture of gibbsite (PDF 76–1782) and bayerite (PDF 20–0011); the former is the main phase. The broad bands at 464, 552, 799, 950, 1093 and 1180 cm^{-1} observed in the IR spectrum of silica[11,12] and the absence of any reflections in the corresponding XRD pattern (not shown) indicate that the hydrous silica used here is an amorphous phase. The exact composition of the reagent mixture was calculated on the basis of thermal analysis, which takes into account the presence of H2O, hydroxide and carbonate.

Synthesis of $La_{9.33}Si_6O_{26}$

The results of milling of the mixture of the parent La_2O_3 and SiO_2 powders corresponding to the $La_{9.33}Si_6O_{26}$ stoichiometry for 35 min are shown in Figure 4 and Figure 5. According to the XRD data (Figure 4), a product of the mechanochemical activation consists primarily of the apatite-structured phase (PDF 49–0443). The reflections for the apatite phase are very broad; this is caused by both small crystallite size and lattice distortion because of the high-power milling. The mean crystallite size calculated from Scherrer's equation is ca 10 nm. Any admixed phases if present are difficult to reveal in the diffraction pattern because of the broad reflections for the apatite phase.

The IR data show (Figure 5) that only small amounts of unreacted SiO_2 (bands at 1087 and 1200 cm^{-1}) and some surface carbonates (wide bands in the region 1386–1485 cm^{-1}) are present in the product along with apatite (bands at 458, 495, 539 cm^{-1} ascribed to the bending modes and a band at 914 cm^{-1} ascribed to the stretching mode of [SiO_4] isolated tetrahedra in the apatite),[8,13] thus indicating that the synthesis reaction for apatite is practically completed in 35 min.

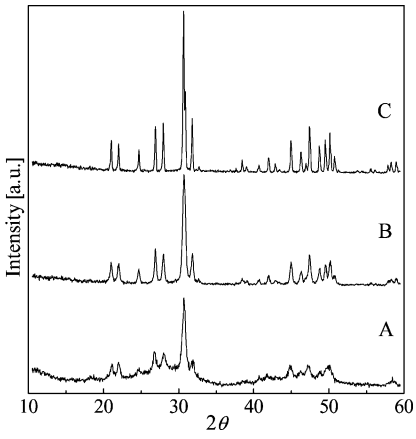

Figure 4. X-ray powder diffraction patterns of the activated SiO_2 + La_2O_3 mixture corresponding to the $La_{9.33}Si_6O_{26}$ composition after (A) milling for 35 min and following calcination at (B) 900 °C and (C) 1200 °C.

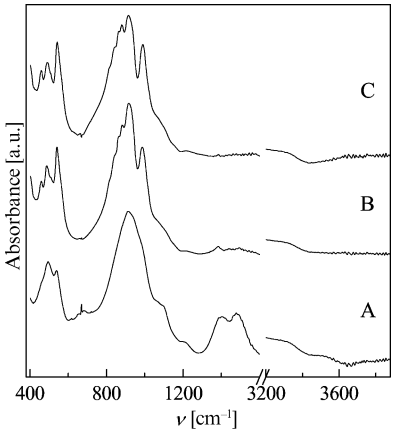

Figure 5. FTIR spectra of the activated SiO_2 + La_2O_3 mixture corresponding to the $La_{9.33}Si_6O_{26}$ composition after (A) milling for 35 min and following calcination at (B) 900 °C and (C) 1200 °C.

According to the literature data,[11] a weak band at 669 cm^{-1} in the IR spectrum of uncalcined $La_{9.33}Si_6O_{26}$ corresponds to Si–O–Si vibrations and may be caused by formation of $[Si_2O_7]$ units in the by-product Si-containing phases or by strong lattice disordering of the apatite phase. However, in the spectra of the calcined sample, this band, as well as those assigned to the CO_3 group and to SiO_2, is not observed (Figure 5). According to the XRD patterns (Figure 4), samples calcined at 900 and 1200 °C are single-phase ATLS; the crystallite size increases with the annealing temperature but remains in the nanorange – 19 nm at 900 °C and 36 nm at 1200 °C. The lattice parameters refined for the sample calcined at 1200 °C (Table 1) are similar to those obtained by Sansom et al.,[3] which suggests the formation of the target phase.

Synthesis of Doped ATLS: Kinetics Study

XRD and TEM Data

The kinetics for the mechanochemical synthesis of ATLS was studied for the mixture of La_2O_3, $Al(OH)_3$ and SiO_2, which corresponds to the $La_{9.83}Si_{4.5}Al_{1.5}O_{26}$ composition. The phase evolution when milling was carried out for 35 min is presented in Figure 6. In the XRD pattern of the starting mixture, reflections for the La_2O_3, $La(OH)_3$ and $La_2O_2CO_3$ phases and weak reflections for $Al(OH)_3$ are

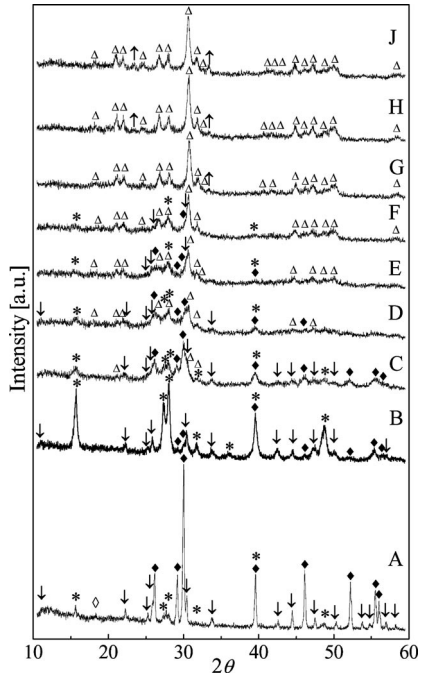

Figure 6. X-ray powder diffraction patterns of the SiO_2 + La_2O_3 + $Al(OH)_3$ mixture corresponding to the $La_{9.83}Si_{4.5}Al_{1.5}O_{26}$ composition before and after milling for different times: (A) starting mixture, (B) 1 min, (C) 5 min, (D) 10 min, (E) 15 min, (F) 20 min, (G) 25 min, (H) 30 min, (J) 35 min; ✧ – $Al(OH)_3$, ♦ – La_2O_3, * – $La(OH)_3$, ↓ – $La_2O_2CO_3$, Δ – apatite, ↑ – $LaAlO_3$.

Table 1. Some characteristics of the sample synthesized after calcination at 1200 °C.

Sample stoichiometry	Phase composition	Apatite stoichiometry[a]	Unit-cell parameters	
			a [Å]	*c* [Å]
$La_{9.33}Si_6O_{26}$	apatite	$La_{9.33}Si_6O_{26}$	9.730(0)	7.194(5)
$La_{9.83}Si_{5.5}Al_{0.5}O_{26.5}$	apatite	$La_{9.83}Si_{5.51}Al_{0.49}O_{26.5}$	9.744(3)	7.209(6)
$La_{9.83}Si_5AlO_{26.25}$	apatite, $LaAlO_3$	$La_{9.90}Si_{5.08}Al_{0.92}O_{26.39}$	9.741(3)	7.218(9)
$La_{9.83}Si_{4.5}Al_{1.5}O_{26}$	apatite, $LaAlO_3$	$La_{9.95}Si_{4.64}Al_{1.36}O_{26.25}$	9.740(6)	7.237(0)
$La_{9.67}Si_5AlO_{26}$	apatite, $LaAlO_3$	–	9.738(0)	7.212(8)
$La_{9.5}Si_{5.5}Al_{0.5}O_{26}$	apatite	$La_{9.5}Si_{5.5}Al_{0.5}O_{26}$	9.744(0)	7.207(4)
$La_{9.42}Si_{5.75}Al_{0.25}O_{26}$	apatite	$La_{9.42}Si_{5.75}Al_{0.25}O_{26}$	9.740(1)	7.201(2)

[a] According to ^{27}Al NMR MAS spectroscopic data.

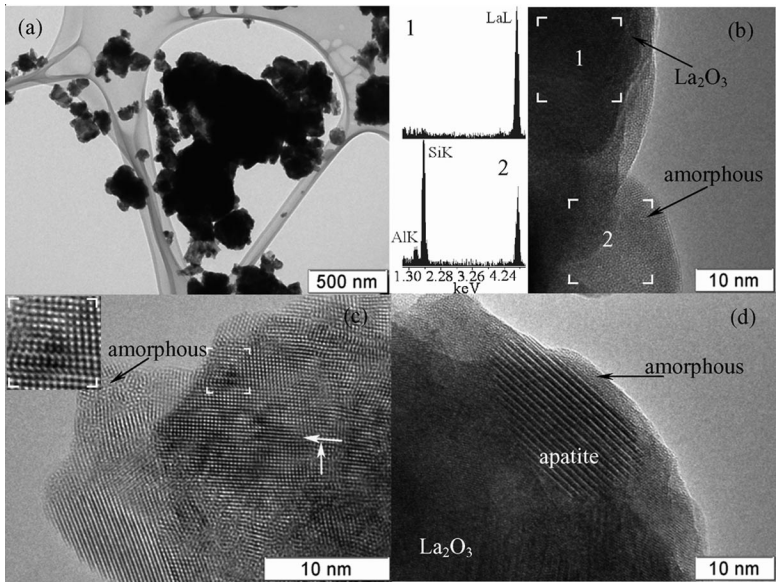

Figure 7. TEM images of the SiO_2 + La_2O_3 + $Al(OH)_3$ mixture corresponding to the $La_{9.83}Si_{4.5}Al_{1.5}O_{26}$ composition after milling for 5 min.

present; La_2O_3 is the main lanthanum-containing phase. After milling for 1 min, the reflections for $La(OH)_3$ become very intense along with a significant decrease in the reflections for La_2O_3. In addition, there are no reflections for the parent $Al(OH)_3$ phase in the pattern.

Further milling results in a decrease in the $La(OH)_3$ peak intensity to practically the same intensity as that before mechanochemical activation – the intensity of the reflections for La_2O_3 increase after treatment for 5 min. The reflections for all phases observed in the pattern of the mixture that was activated for 5 min are broad, which is mainly caused by a significant lattice distortion during the first stage of milling. Thus, TEM images show that after activation for 5 min a sample consists of big (≈200 nm) crystalline La_2O_3 particles and agglomerates (≈1 μm) of the La_2O_3 and Si-based amorphous particles (Figure 7a–c). The lanthanum oxide particles are shown to be highly disordered, and are composed of crystallites with a size of about 10 nm (Figure 7c).

Another interesting fact that arises from the XRD pattern is that milling for 5 min with a rotation speed of 1200 rpm may be sufficient to initiate ATLS formation. In the corresponding XRD pattern, there is a new weak reflection at 21.1° (2θ) that may be the {200} line of lanthanum silicate. Other reflections for apatite overlap with those for the parent phases. The transmission microscopy data confirm this suggestion, which indicates the formation of the apatite phase (Figure 7d).

After milling for 10 min, the reflections for the apatite phase become more evident, and the intensities of the reflections for La_2O_3 decrease detectably. After milling for 20 min, apatite is the main phase; however, some amounts of La_2O_3 and $La(OH)_3$ are still present. Reflections for the latter phase disappear after mechanochemical activation for 25 min. However, new reflections for the $LaAlO_3$ phase (PDF 31–0022) first appear at 33.4° after milling for 25 min and then also at 23.4° after 30 min of activation.

After milling for 35 min, only reflections for the apatite and $LaAlO_3$ phases are present in the XRD pattern. High resolution TEM micrographs of the sample after 35 min of activation (Figure 8) shows that it comprises well-ordered nanoparticles (10–60 nm) and their micron-sized agglomer-

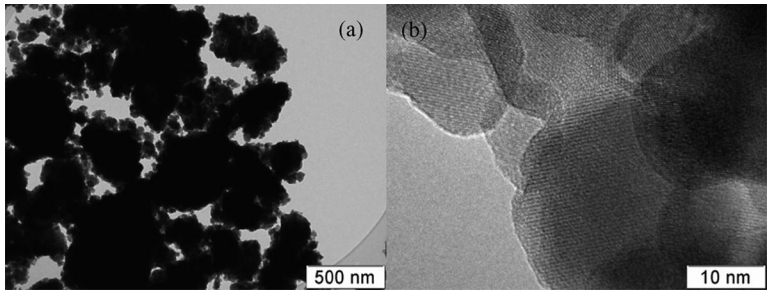

Figure 8. TEM images of the SiO_2 + La_2O_3 + $Al(OH)_3$ mixture corresponding to the $La_{9.83}Si_{4.5}Al_{1.5}O_{26}$ composition after milling for 35 min.

ates. The apatite nanoparticles with sizes of 30–60 nm are shown to be formed by the stacking of nanocrystallites with sizes of 10–15 nm.

IR Spectroscopy Data

An IR spectroscopic study of the formation of ATLS gives new information that completes the XRD data. The IR spectra of the starting mixture and that after milling are shown in Figure 9. A band at ≈912 cm^{-1} attributed to the asymmetric stretching vibrations of the Si–O band in isolated SiO_4 tetrahedra of apatite, which is absent in the spectrum of the initial mixture, appears in the spectrum of the mixture that has been milled for 5 min, and its intensity increases with further activation. Moreover, a weak band in this region is observed already after milling for 1 min, which suggests that changes have begun to take place in the short-range structure of the parent SiO_2. However, the IR data show that apatite formation is completed only after milling for 35 min. The spectra of the sample after milling for a shorter time contain bands assigned to unreacted SiO_2, La_2O_3 or $La(OH)_3$.

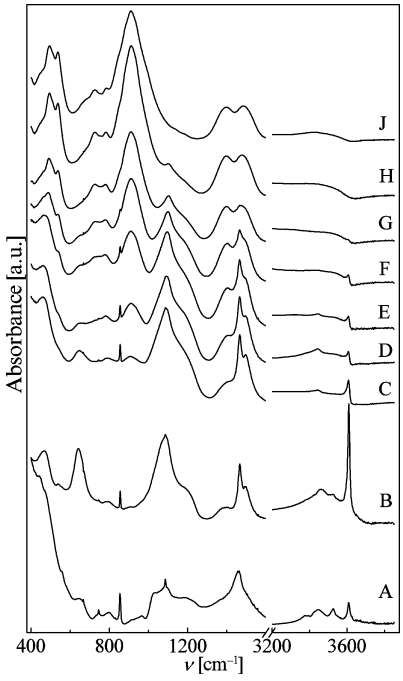

Figure 9. FTIR spectra of the SiO_2 + La_2O_3 + $Al(OH)_3$ mixture corresponding to the $La_{9.83}Si_{4.5}Al_{1.5}O_{26}$ composition before and after milling for different times: (A) start mixture, (B) 1 min, (C) 5 min, (D) 10 min, (E) 15 min, (F) 20 min, (G) 25 min, (H) 30 min, (J) 35 min.

According to the IR data, which is in agreement with the XRD data, La_2O_3 (a strong band assigned to the La–O mode at 400–600 cm^{-1}) converts to $La(OH)_3$ after activation for 1 min, but further milling causes a significant decrease in the amount of $La(OH)_3$ (bands at 643, 3610 cm^{-1}), and again the band intensity of La_2O_3 increases. However, some $La(OH)_3$ is present in the mixture even after milling for 25 min, which is indicated by the presence of a weak band at 3610 cm^{-1} (Figure 9).

Further, the IR data show that milling for 1–5 min results in the perceptible transformation of the parent $Al(OH)_3$. Thus, a strong band at 1023 cm^{-1} assigned to the Al–O mode disappears, and some changes in the main band of SiO_2 (Si–O stretching vibrations with a maximum at 1093 cm^{-1}) are observed as well. In the region of the OH stretching vibrations, a band at 3448 cm^{-1} shifts to ca. 3463 cm^{-1} after milling for 1 min, but after further activation, it appears at 3448 cm^{-1} again, and disappears completely only in the spectrum of the sample milled for 20 min. The other bands for the Al–OH modes in this region already disappear after 5 min of activation, and a wide band for the OH stretching modes in H_2O appears. These data suggest the formation of an amorphous aluminium silicate,[11] which is confirmed by EDX analysis of the amorphous particles (Figure 7b). The latter indicates that the amorphous phase observed is not just silica, but contains both Al and Si atoms.

Further activation results in new bands at 782 and 726 cm^{-1}, which are attributed to the Al–O modes in $[AlO_4]$, that appear concurrently with the rise in the intensity of the apatite bands. This suggests the formation of Al-doped apatite. The additional shoulder at ca. 677 cm^{-1} that appears after milling for 25 min indicates, in accordance with the XRD data, the formation of $LaAlO_3$ containing Al cations in the octahedral coordination.[11,14]

Finally, the IR study shows changes in $La_2O_2CO_3$ that is present in the parent lanthanum oxide. Thus, the spectrum of the reagent mixture before activation and that of the parent lanthanum oxide contain bands corresponding to the vibrations of the CO_3 group in the crystalline carbonate (in particular, a single band at 1464 cm^{-1}). The mechanochemical treatment results in significant changes in the spectra in the region 1386–1485 cm^{-1} assigned to the carbonates, which reflects the formation of surface carbonates (broad bands at 1400 and 1490 cm^{-1}) along with the formation of apatite.

^{27}Al and ^{29}Si MAS NMR Spectroscopic Study

For a better understanding of the process for the formation of the ATLS structure, ^{29}Si and ^{27}Al MAS NMR spectroscopy was used (Figure 10). In the ^{29}Si MAS NMR spectrum (79.4 MHz, ν_r = 8 kHz, 25 °C) of starting SiO_2, two overlapping peaks at δ = –109.8 and –102.1 ppm corresponding to $[SiO_4]$ tetrahedrons of Q^4 and Q^3 types are observed.[15] Milling of the initial mixture for 5 min results in the broadening of these peaks, which suggests distortion of the local structure of silica. The appearance of the signal at δ = –77.2 ppm, typical for isolated $[SiO_4]$ tetrahedra (Q^0 type), indicates the beginning of the formation of apatite,[15,16] which agrees with the XRD and IR data. After milling for 20 min, the ^{29}Si MAS NMR spectrum shows a single signal at δ = –77.2 ppm, which characterizes the apatite phase. Subsequent increase in the milling time to up to 35 min is accompanied by line broadening, thus indicating the distortion of the apatite structure.

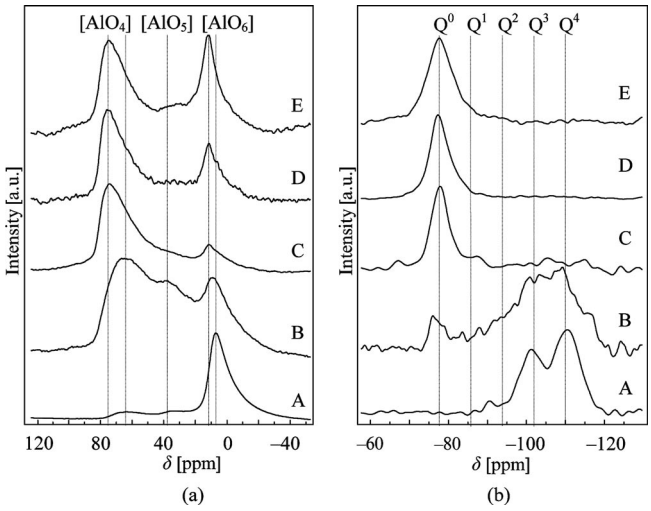

Figure 10. (a) ^{27}Al NMR MAS spectra (104.2 MHz, ν_r = 10 kHz, 25 °C) and (b) ^{29}Si NMR MAS (79.4 MHz, ν_r = 8 kHz, 25 °C) spectra of (A) parent $Al(OH)_3$ and SiO_2, respectively, and of the $SiO_2 + La_2O_3 + Al(OH)_3$ mixture corresponding to the $La_{9.83}Si_{4.5}Al_{1.5}O_{26}$ composition after milling for different times: (B) 5 min, (C) 20 min, (D) 30 min, (E) 35 min.

In the ^{27}Al MAS NMR spectrum (104.2 MHz, ν_r = 10 kHz, 25 °C) of starting $Al(OH)_3$, the characteristic peak at δ = 7.5 ppm, corresponding to octahedral [AlO_6] units, is present.[15] Broad signals at δ = 63 and 38.5 ppm, assigned to tetrahedral [AlO_4] and five-coordinate [AlO_5] units, respectively, which appear in the ^{27}Al MAS NMR spectrum after 5 min of mechanochemical treatment, imply the formation of an amorphous Al/Si-containing phase.[15,17] This confirms the suggestion based on the IR and TEM data. According to the ^{27}Al MAS NMR spectra of the sample that was activated for 20 min, a rise in the [AlO_4] content and the disappearance of [AlO_5] and [AlO_6] units are observed. The signal at δ = 75.5 ppm, assigned to tetrahedral [AlO_4] units, is somewhat different from that observed in the spectrum recorded after milling for 5 min; this may be related to the incorporation of Al into Si sites in the formed apatite phase. Simultaneously, a new peak at δ = 11.5 ppm, corresponding to octahedral [AlO_6] units of $LaAlO_3$, appears and grows with further activation,[15] which indicates that only a part of Al could be incorporated into the apatite structure for the mixture corresponding to the $La_{9.83}Si_{4.5}Al_{1.5}O_{26}$ composition.

Mechanism of Formation of Apatite

There are different ways of chemical interaction between solid compounds during mechanochemical treatment. The interaction may be affected by many factors, including chemical composition, structure, particle size, hardness and disordering of reagents, reaction medium, etc. For the most part, formation of new compounds during mechanochemical synthesis occurs through the amorphous state of all reagents followed by crystallization of the target phase.[9,12,18] However, when the reagents and product have similar structures, the cluster-topotactic mechanism, where the product is formed on the surface of the initial matrix, is possible.[12]

As pointed out previously, La_2O_3 is characterized by the hexagonal lattice belonging to the $P\bar{3}m1$ space group (PDF 05–0602; a = 3.9373 Å, c = 6.1299 Å). The apatite formed also has a hexagonal lattice that belongs to the $P6_3/m$ space group. The lattice parameters estimated for the calcined Al-doped sample are a = 9.712(8) Å and c = 7.185(8) Å (Table 1). In addition, the $La(OH)_3$ observed has a hexagonal lattice that belongs to the same space group ($P6_3/m$; PDF 36–1481) as that of apatite. According to PDF 36–1481, the lattice parameters of $La(OH)_3$ are a = 6.5286 Å and c = 3.8588 Å, which are similar to those of La_2O_3. Such structural similarity could favour the cluster-topotactic mechanism of ATLS formation.

The kinetic features of the mechanochemical synthesis of ATLS studied by XRD, TEM, and IR and NMR spectroscopy (vide supra) agree with the cluster-topotactic mechanism of its formation. First of all, in spite of strong disordering, La_2O_3 remains crystalline during the milling process until its complete consumption. Further, IR and XRD data show that both reagent and product phases are simultaneously present in the mixture during the process. Therefore, the formation of the apatite phase does not proceed through its crystallization from an amorphous matrix.

According to the XRD and IR data, during the first stage of activation, the transition of La_2O_3 to $La(OH)_3$ due to hydration is observed, followed by a decrease in the $La(OH)_3$ phase content and an increase in that of La_2O_3. As can be seen in the TEM images, which are supported by EDX spectra (Figure 7b), amorphous SiO_2 (or aluminosilicate) begins to cover the crystalline particles. Hydrous silica, as a weak acid, appears to react with basic $La(OH)_3$ and covers the La_2O_3 particles to form a lanthanum silicate. The latter is confirmed by the appearance of a band attributed to Si–O vibrations in isolated SiO_4 tetrahedra in the IR spectrum and a Q^0 type signal for Si in the ^{29}Si NMR MAS spectrum already after milling for 5 min (vide supra). Such an abrupt La_2O_3 transformation into $La(OH)_3$ followed by a decrease in the $La(OH)_3$ content and easy apatite formation during the first 1–5 min of milling is typical for soft mechanochemical synthesis involving hydration and acid–base reactions.[19]

The La_2O_3 with a hexagonal structure may play a role of the initial matrix for the topotactic growth of the emerging apatite; in so doing, strong disordering of the La_2O_3 lattice favours apatite cluster formation on its surface (Figure 7c, d). Such clusters of a new phase apparently play the role of nuclei for its further crystallization, which results in the formation of nanostructured apatite particles, as can be seen from the TEM data (Figure 8).

Comparison of the XRD patterns for undoped and Al-doped samples after milling for 20 min (Figure 6 and Figure 11) suggests that the presence of $Al(OH)_3$ in the starting mixture promotes apatite formation. Thus, after milling for 1 min, the mixture corresponding to the $La_{9.33}Si_6O_{26}$ composition as well as that of the Al-doped sample contains mainly the $La(OH)_3$ phase. In contrast to the Al-doped sample, apatite formation for the undoped sample is not complete even after activation for 20 min. This may be

caused by the formation of an aluminosilicate as a result of the acid–base reaction between $Al(OH)_3$ and SiO_2 during activation, as was shown by Klevtsov et al.[17] The IR and ^{27}Al MAS NMR data of the Al-doped sample that was milled for 5 min confirm such aluminosilicate formation (vide supra). As it is a stronger acid than silica,[20] aluminosilicate could favour the acid–base reaction for apatite formation by soft mechanochemical synthesis. On the other hand, the presence of $Al(OH)_3$ results in the formation of a secondary $LaAlO_3$ phase.

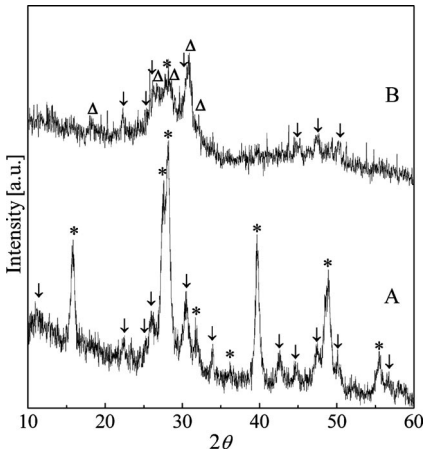

Figure 11. X-ray powder diffraction patterns of the SiO_2 + La_2O_3 mixture corresponding to the $La_{9.33}Si_6O_{26}$ composition after milling for different times: (A) 5 min, (B) 20 min; * – $La(OH)_3$, ↓ – $La_2O_2CO_3$, Δ – apatite.

Influence of Al Concentration on Phase Composition

A range of Al-doped ATLS with different Al content was synthesized by mechanochemical activation for 20 min followed by calcination at 1200 °C to investigate the possibility of Al-doping. The results are presented in Table 1. According to these data, some $LaAlO_3$ can be formed along with apatite. The ^{27}Al MAS NMR data (104.2 MHz, ν_r = 10 kHz, 25 °C) testify that for biphasic samples Al is present in both phases: δ = 75.5 ppm assigned to tetrahedral $[AlO_4]$ units in the apatite phase and δ = 11.5 ppm corresponding to octahedral $[AlO_6]$ units in the $LaAlO_3$ phase (Figure 12a).[15] The apatite composition depends on the amount of Al incorporated into silicate and on lanthanum content in the sample, which determines the concentration of vacancies in the cation sublattice and the oxygen excess. According to the ^{29}Si MAS NMR (79.4 MHz, ν_r = 8 kHz, 25 °C) data (Figure 12b), different environments of silicon exist in some samples. The peak at δ = 77.0 ppm corresponds to $[SiO_4]$ tetrahedrons of the Q^0 type, while those at δ = 81.0 and 84.5 ppm seem to be due to $[SiO_4]$ tetrahedrons of Q^1 type.[15,16] The same features for apatite-type silicates were reported by Sansom et al., who suggest that they correspond to local distortions caused by the presence of cation vacancies and interstitial oxide ion defects.[16] The ^{27}Al MAS NMR and ^{29}Si MAS NMR data (Table 1) suggest that cation vacancies favour association of two $[SiO_4]^{4-}$ groups, which leads to the additional formation of some interstitial oxygen species.

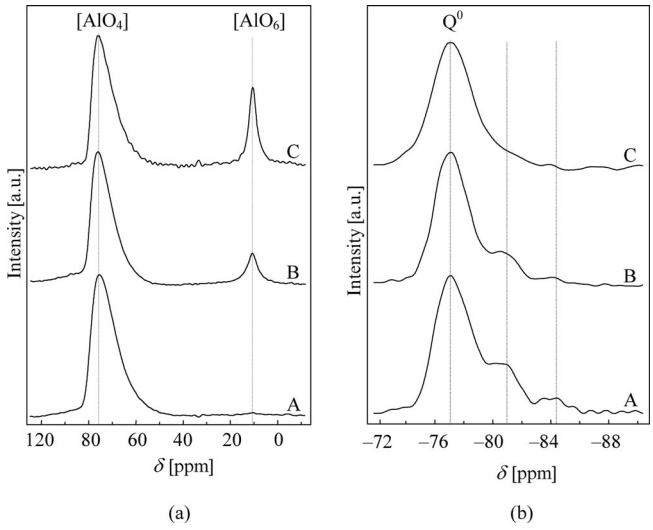

Figure 12. (a) ^{27}Al NMR MAS (104.2 MHz, ν_r = 10 kHz, 25 °C) and (b) ^{29}Si NMR MAS (79.4 MHz, ν_r = 8 kHz, 25 °C) spectra of (A) $La_{9.83}Si_{5.5}Al_{0.5}O_{26.5}$, (B) $La_{9.83}Si_5AlO_{26.25}$ and (C) $La_{9.83}Si_{4.5}Al_{1.5}O_{26}$ calcined at 1200 °C.

The secondary phase formation may be caused either by a limited substitution of $[SiO_4]$ with $[AlO_4]$ in the apatite structure or by the action of high-power mechanochemical treatment, which may result in both synthesis and destruction.[12,21] It was reported that a dynamic mechanochemical equilibrium may be established in the mixtures under the milling process, if different stable phases can form.[6] The octahedral coordination for Al is more typical than the tetrahedral one. Therefore, an equilibrium between the apatite phase containing Al with a tetrahedral coordination and $LaAlO_3$, in which Al has an octahedral environment, could exist.

As indicated above for the sample with the $La_{9.83}Si_{4.5}Al_{1.5}O_{26}$ composition, the reflections for the $LaAlO_3$ phase appear in the XRD patterns after milling for 25 min. However, according to the ^{27}Al MAS NMR data, some $LaAlO_3$ is already present in the mixture after activation for 20 min. For a better understanding of the nature of formation of $LaAlO_3$, the mixture corresponding to the $La_{9.83}Si_{4.5}Al_{1.5}O_{26}$ composition after milling for 5, 20 and 30 min was calcined at 900 and 1200 °C (Figure 13, Figure 14 and Figure 15). According to the XRD data, calcination of the sample after activation for 35 min at 1200 °C for 5 h does not result in the disappearance of the perovskite phase (Figure 15). The patterns of the samples activated for 5 and 20 min and calcined at 1200 °C also contain reflections for the $LaAlO_3$ phase, though apatite forms through different routes. According to the XRD and IR spectroscopic data (not shown), in the case for the sample that was activated for 5 min, the formation of the apatite phase occurs through a solid-state reaction route, and primarily the apatite phase with a small admixture of the $LaAlO_3$ phase forms only at 1200 °C (Figure 13). In the case for the sample activated for

20 min, as was noted before, the apatite phase is the main phase already after milling, and calcination at 900 °C results in practically the formation of single-phase apatite (Figure 14). In addition, the intensity of the reflections for the perovskite phase in the XRD pattern of the sample that was activated for 5 min is lower than those in the pattern of the sample that was activated for 35 min and calcined at 1200 °C for 5 h. However, the former was shown to increase with calcination for longer times (10 h), which may be caused by structure ordering and the slow approaching to thermodynamic equilibrium.

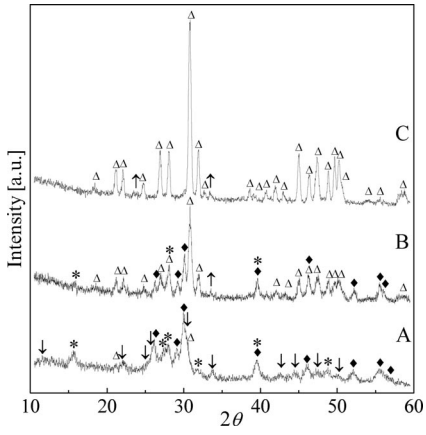

Figure 13. X-ray powder diffraction patterns of the SiO_2 + La_2O_3 + $Al(OH)_3$ mixture corresponding to the $La_{9.83}Si_{4.5}Al_{1.5}O_{26}$ composition after milling for 5 min: (A) as milled, (B) calcined at 900 °C, (C) calcined at 1200 °C; ♦ – La_2O_3, * – $La(OH)_3$, ↓ – $La_2O_2CO_3$, Δ – apatite, ↑ – $LaAlO_3$.

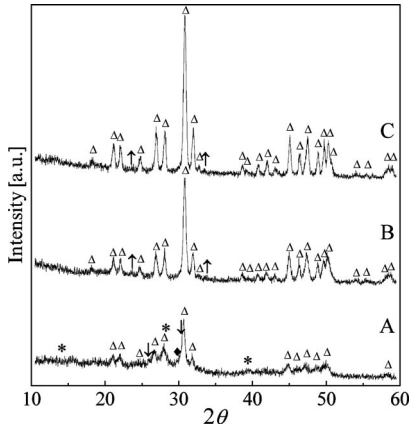

Figure 14. X-ray powder diffraction patterns of the SiO_2 + La_2O_3 + $Al(OH)_3$ mixture corresponding to the $La_{9.83}Si_{4.5}Al_{1.5}O_{26}$ composition after milling for 20 min: (A) as milled, (B) calcined at 900 °C, (C) calcined at 1200 °C; ♦ – La_2O_3, * – $La(OH)_3$, ↓ – $La_2O_2CO_3$, Δ – apatite, ↑ – $LaAlO_3$.

Thus, the present data suggest that the formation of $LaAlO_3$ is mainly caused by limited substitution of Si by Al in the apatite structure, and there is some domain in the La_2O_3–SiO_2–Al_2O_3 phase diagram at room temperature in which the Al-doped apatite and $LaAlO_3$ phases coexist and in which apatite apparently forms a continuous range of solid solution $La_{9.33+x/3+y}Si_{6-x}Al_xO_{26+3y/2}$ (x = 0–1.5, y = 0–0.67). The upper limit of the incorporation of Al into apatite may be higher than the value pointed out in this study (Table 1), which is determined by the domain boundaries. Further, as is evident from the kinetic study, mechanochemical treatment may affect both the formation and destruction of doped apatite, which results in the establishment of a mechanochemical dynamic equilibrium, which may correspond to or be near the thermodynamic equilibrium.

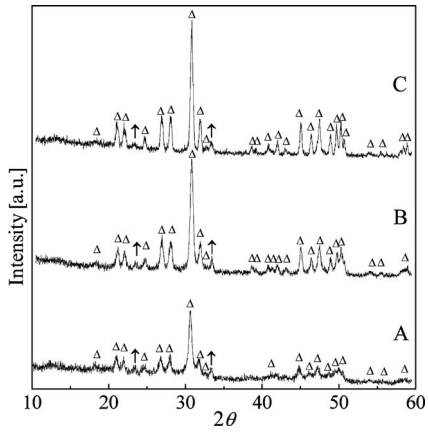

Figure 15. X-ray powder diffraction patterns of the SiO_2 + La_2O_3 + $Al(OH)_3$ mixture corresponding to the $La_{9.83}Si_{4.5}Al_{1.5}O_{26}$ composition after milling for 35 min: (A) as milled, (B) calcined at 900 °C, (C) calcined at 1200 °C; Δ – apatite, ↑ – $LaAlO_3$.

Conclusions

The mechanochemical synthesis of Al-doped ATLS has been described. The lanthanum silicates were successfully prepared at room temperature by using a high-power (1200 rpm) ball mill, which primarily favours the formation of the apatite phase already after activation for 20–35 min. The data obtained indicate a cluster-topotactic mechanism for the synthesis of the lanthanum silicates, which involves hydration of the reagents and acid–base reactions. La_2O_3 with a hexagonal structure is suggested to be an initial matrix for the topotactic growth of apatite. Strong disordering of the La_2O_3 lattice favours the formation of apatite clusters on its surface, which play the role of nuclei for further crystallization to form nanocrystalline apatite particles. Al-doping results in the formation of aluminosilicate, which promotes that of the apatite. The formation of a secondary phase of $LaAlO_3$, which depends on the sample stoichiometry, suggests the existence of a biphase domain in the La_2O_3–SiO_2–Al_2O_3 phase diagram at room temperature.

Experimental Section

$Al(OH)_3$ (REACHIM, 99.5%), La_2O_3 (VEKTON, 99.99%) and SiO_2 (REACHIM, 99.9%) were used as parent compounds to synthesize ATLS. The stoichiometric mixtures of the starting materials were activated in a high-power planetary ball mill AGO-2 (steel ball diameter 8 mm; steel drum volume 150 mL; rotation rate 1200 rpm; sample-to-ball mass ratio 1/20). Samples were activated for 1–

35 min for the kinetic study and for 20 min (to prevent destruction of the apatite structure as a result of mechanochemical treatment) for the preparation of doped samples with different Al content. Unless specially stated, the products of MA were calcined at 900 and 1200°C for 5 h.

Thermal analysis of the starting compounds was carried out with a Q-1500D thermoanalyzer. The phase composition of the parent compounds and samples prepared was examined by using powder X-ray diffraction. XRD patterns were obtained with URD-6M or Dron-3M diffractometers by using Cu-K_α radiation with a secondary monochromator. TEM studies were performed on a JEM-2010 with EDX Phoenix Spectrometer equipped with Si (Li) detector. IR spectra were recorded with a Shimadzu FTIR-8300 spectrometer by using KBr pellets. ^{27}Al MAS NMR (104.2 MHz, ν_r = 10 kHz, 25 °C) and ^{29}Si MAS NMR (79.4 MHz, ν_r = 8 kHz, 25 °C) data were collected by using a Bruker Avance-400 spectrometer operating with a 4-mm MAS probe. ^{29}Si and ^{27}Al chemical shifts are referred to external $SiMe_4$ and $Al(H_2O)_6^{3+}$ standards, respectively. Estimation of the stoichiometry of the apatite was made by considering the distribution of Al between the apatite and $LaAlO_3$ phases. The latter was calculated from ^{27}Al MAS NMR data on the basis of the proportionality between the peak integral in the NMR spectrum and the number of atoms. The Fe impurity caused by using steel drums and balls was analyzed with a Optical Atomic Emission Spectrometer Optima 4300DV; the amount of Fe impurity in the samples after 25 min of MA was less then 0.05 ± 0.01 w.-%.

Acknowledgments

The authors gratefully acknowledge the support provided through the European Commission 6th Framework Programme within the Novel Materials for Silicate-Based Fuel Cells Project.

[1] a) S. Nakayama, H. Aono, Y. Sadaoka, *Chem. Lett.* **1995**, *6*, 431–432; b) S. Nakayama, T. Kageyama, H. Aono, Y. Sadaoka, *J. Mater. Chem.* **1995**, *5*, 1801–1805; c) S. Nakayama, M. Sakamoto, *J. Eur. Ceram. Soc.* **1998**, *18*, 1413–1418.

[2] a) R. K. B. Gover, P. R. Slater, *Annu. Rep. Prog. Chem. Sect. A Inorg. Chem.* **2003**, *99*, 477–504; b) J. E. H. Sansom, P. Slater, *Annu. Rep. Prog. Chem. Sect. A Inorg. Chem.* **2005**, *101*, 489–512.

[3] a) J. E. H. Sansom, D. Richings, P. R. Slater, *Solid State Ionics* **2001**, *139*, 205–210; b) E. Kendrick, M. S. Islam, P. R. Slater, *J. Mater. Chem.* **2007**, *17*, 3104–3111.

[4] a) E. J. Abram, D. C. Sinclair, A. R. West, *J. Mater. Chem.* **2001**, *11*, 1978–1979; b) A. Najib, J. E. H. Sansom, J. R. Tolchard, P. R. Slater, M. S. Islam, *Dalton Trans.* **2004**, 3106–3109; c) A. L. Shaula, V. V. Kharton, F. M. B. Marques, *J. Solid State Chem.* **2005**, *178*, 2050–2061; d) J. E. H. Sansom, E. Kendrick, J. R. Tolchard, M. S. Islam, P. R. Slater, *J. Solid State Electrochem.* **2006**, *10*, 562–568; e) T. Kharlamova, S. Pavlova, V. Sadykov, O. Lapina, D. Khabibulin, T. Kriger, V. Zaikovskii, A. Ishchenko, A. Salanov, V. Muzykantov, N. Mezentseva, M. Chaikina, N. Uvarov, J. Frade, Ch. Argirusis, *Solid State Ionics*, in press.

[5] a) L. Leon-Reina, E. R. Losilla, M. Martınez-Lara, S. Bruque, A. Llobet, D. V. Sheptyakovc, M. A. G. Aranda, *J. Mater. Chem.* **2005**, *15*, 2489–2498; b) H. Yoshioka, *J. Alloys Compd.* **2006**, *408–412*, 649–652.

[6] V. Zyrynov, *Interceram* **2003**, *52*, 22–27; b) V. V. Zyryanov, *Science of Sintering* **2005**, *37*, 77–92.

[7] a) S. W. Tao, J. T. S. Irvine, *Ionics* **2000**, *6*, 389–396; b) S. Tao, J. T. S. Irvine, *Mater. Res. Bull.* **2001**, *36*, 1245–1258; c) S. Celerier, C. Laberty, F. Ansart, P. Lenormand, P. Stevens, *Ceram. Int.* **2006**, *32*, 271–276; d) S. Celerier, C. Laberty-Robert, F. Ansart, C. Calmet, P. Stevens, *J. Eur. Ceram. Soc.* **2005**, *25*, 2665–2668.

[8] a) A. F. Fuentes, E. Rodriguez-Reyna, L. G. Martinez-Gonzalez, M. Maczka, J. Hanuza, U. Amador, *Solid State Ionics* **2006**, *177*, 1869–1873; b) E. Rodriguez-Reyna, A. F. Fuentes, M. Maczka, J. Hanuza, K. Boulahya, U. Amador, *J. Solid State Chem.* **2006**, *179*, 522–531.

[9] a) E. G. Avvakumov, *Mechanical Methods in Chemical Processes Activation*, Nauka, Novosibirsk, **1986**, p. 303; b) E. G. Avvakumov (Ed.), *Mechanochemical Synthesis in Inorganic Chemistry*, Nauka, Novosibirsk, **1999**.

[10] G. Tzvetkov, N. Minkova, *Mater. Lett.* **1999**, *39*, 354–358.

[11] I. I. Plusnina, *Infrared Spectra of Silicates*, Moscow University, **1967**, p. 90.

[12] M. V. Chaikina, *Mechanochemistry of Natural and Synthetic Apatites* (Ed.: E.G. Avvakumov), Publishing House of SB RAS, Branch GEO, Novosibirsk, **2002**, p. 223.

[13] R. E. Ouenzerfia, C. Goutaudiera, G. Panczera, B. Moinea, M. T. Cohen-Adada, M. Trabelsi-Ayedib, N. Kbir-Ariguib, *Solid State Ionics* **2003**, *156*, 209–222.

[14] P. R. Aravind, P. Mukundan, P. K. Pillai, K. G. K. Warrier, *Microporous Mesoporous Mater.* **2006**, *96*, 14–20.

[15] a) G. Engelhardt, D. Michel, *High-Resolution Solid-State NMR of Silicates and Zeolites*, John Wiley & Sons, **1987**, pp. 97; b) R. Dupree, M. H. Lewis, M. E. Smith, *J. Am. Chem. Soc.* **1989**, *111*, 5125–5132; c) T. Isobe, T. Watanabe, J. B. d′Espinose de la Caillerie, A. P. Legrand, D. Massiot, *J. Colloid Interface Sci.* **2003**, *261*, 320–324.

[16] J. E. H. Sansom, J. R. Tolchard, M. S. Islam, D. Apperley, P. R. Slater, *J. Mater. Chem.* **2006**, *16*, 1410–1413.

[17] a) D. P. Klevtsov, O. P. Krivoruchko, V. M. Mastikhin, E. A. Paukshtis, B. P. Zolotovskii, R. A. Buyanov, *Izv. Sib. Otd. Akad. Nauk, Ser. Khim. Nauk* **1988**, *3*, 70–77 (in Russian); b) D. P. Klevtsov, B. P. Zolotovskii, O. P. Krivoruchko, R. A. Buyanov, *J. Appl. Chem.* **1988**, *61*, 914–916.

[18] G. Heinicke, *Tribochemistry*, Academ-Verlag, Berlin, **1984**.

[19] a) E. Avvakumov, M. Senna, N. Kosova, *Soft Mechanochemical Synthesis: A Basis for New Chemical Technologies*, Kluwer Academic Publishers, **2001**, p. 207; b) E. G. Avvakumov, E. T. Devyatkina, N. V. Kosova, *J. Solid State Chem.* **1995**, *113*, 379–383.

[20] I. D. Micheikin, *Soros Educational J.* **2001**, *5*, 43–50.

[21] D. Mazza, S. Ronchetti, *Mater. Res. Bull.* **1999**, *34*, 1375–1382.

Received: September 14, 2007
Published Online: January 10, 2008

